Structure and stability of the modulated phase Sb-II

U. Schwarz, L. Akselrud, H. Rosner, Alim Ormeci, and Yu. Grin
Max-Planck-Institut für Chemische Physik fester Stoffe, Nöthnitzer Strasse 40, 01187 Dresden, Germany

M. Hanfland
ESRF, BP220, 38043 Grenoble, France

(Received 4 September 2002; revised manuscript received 19 December 2002; published 9 June 2003)

The crystal structure of Sb-II has been determined using angle-dispersive x-ray diffraction of synchrotron radiation. The crystal structure comprises an interpenetrating assembly of a tetragonal host sublattice with symmetry $I422$ and a tetragonal guest sublattice of symmetry $I422$, which realize common a axes but different c axes. Weak extra peaks that are also reported in recent investigations performed independently are attributed to modulation waves of the atomic positions in both sublattices. A refinement using full profiles of powder-diffraction data was performed in the four-dimensional superspace group $L^{I422}_{-111}:L^{I422}_{-111}$. The structural investigation is accompanied by *ab initio* full-potential band-structure calculations confirming the experimentally determined modification sequence. Fitting equations of state to the results of these computations generates pressure-volume relations which are in excellent agreement with the experimental data. On the basis of total-energy calculations, an earlier proposed crystal structure of the tetragonal phase has to be reconsidered in the light of the composite arrangement in Sb-II.

DOI: 10.1103/PhysRevB.67.214101 PACS number(s): 61.50.Ks, 62.50.+p

I. INTRODUCTION

Pressure-induced structural changes of antimony are a topic of both experimental and theoretical interest for more than 60 years.[1–3] At low pressures, Sb is isotypic to the ambient pressure phases of arsenic as well as bismuth and realizes a rhombohedral crystal structure, so-called $A7$, which is commonly classified as a distortion of a cubic primitive atomic arrangement. At a pressure of 8.5(5) GPa, antimony undergoes a reversible transformation into the high-pressure modification Sb-II. Further increase of pressure induces a transition into a cubic body-centered arrangement of antimony atoms at about 28 GPa.[4] The crystal structure of the high-pressure phase Sb-II is a long-standing matter of controversy and has been reported to be hexagonal, monoclinic, or tetragonal.[5–7] A tetragonal model ($P=12$ GPa, space group $P4/n$, $a=796.5$ pm, $c=385.7$ pm) has been refined using powder-diffraction data and resulted in a model with one type of Sb atom building up a three-dimensional framework and a second kind occupying the resulting channels.[8] A similar self-hosting assembly is assigned to the high-pressure phase of bismuth which is stable between 2.7 GPa and 7.7 GPa.[7,9–11] A recent reinvestigation using a combination of x-ray single crystal and powder-diffraction methods evidences that the crystal structure of Bi is more complex, since the identity periods along the c axes of channel atoms and tetragonal framework are incommensurate with respect to each other. A similar organization is reported for Sb-II, but the proposed model does not account for several weak reflections observed in the experimental profiles.[12]

Electronic structure calculations represent a powerful tool to complement experimental structure determinations. Band-structure calculation techniques are helpful as a guide in determining the correct atomic arrangement by comparing energies for different lattice parameters, internal coordinates, and even different structure types.[13–16] The dependence of physical properties on external or chemical pressure can be simulated reliably by modern full-potential calculations.

We report a full-profile refinement of the atomic arrangement of Sb-II using a four-dimensional superspace group description of the host-guest assembly, which additionally takes into account first-order modulation waves in both sublattices. The experimental results are accompanied by *ab initio* band-structure calculations using two independent full-potential computational schemes to calculate the energy-volume curves for the different phases under discussion. Equations of state are fitted to the results and will be compared with the experimental data.

II. EXPERIMENT

Experiments were performed with antimony samples of 99.999% purity (ABCR Chemicals, Karlsruhe, Germany). Angle-dispersive x-ray powder-diffraction diagrams were measured at ID-9 of the ESRF using an image plate detector and monochromatic radiation with a wavelength of 41.733 pm. Polycrystalline samples were obtained by thorough grinding of antimony granules at ambient conditions. The particles were placed in a gasketed diamond anvil high-pressure cell using a small sphere of ruby for pressure calibration and a 4:1 mixture of methanol and ethanol as a pressure transmitting medium. In order to improve the powder average, samples were oscillated by 3° during exposures of typically 20-s duration. The resulting two-dimensional powder-diffraction images were integrated azimuthally to yield one-dimensional intensity versus 2Θ data.[17] Crystallographic calculations were performed with the program package WINCSD in $(3+1)$-dimensional space mode.[18]

III. CALCULATION METHODS

To account for the difficulties and the possible inaccuracies related to the comparison of electronic structure results

for crystal structures with different symmetries, we used two independent full-potential schemes which are based on the local-density approximation: A full-potential linear muffin-tin orbital (FPLMTO) method and a full-potential nonorthogonal local-orbital (FPLO) code.[19,20] For exchange and correlation potentials, the Perdew-Wang parametrization was employed.[21]

In the FPLMTO method, the basis functions, electron density, and potential were expanded in spherical harmonics with a cutoff $l_{max}=6$ inside the nonoverlapping spheres, and in Fourier series within the interstitial region. The highest core states, $4s$, $4p$, and $4d$, were included in the basis set. Each of these semicore states was represented by two basis functions (double-kappa basis). The valence states were accounted for by a triple-kappa basis. Orthogonality between the semicore and the valence states was ensured by using two sets of energy parameters, one set for each group. The resulting basis formed a single, fully hybridizing basis set. For Brillouin-zone integrations, the special **k**-point method with a Gaussian broadening of width 2.5 mhartree was utilized.[22]

In the FPLO code, Sb $(4p,4d,5s,5p,5d)$ functions were chosen as the basis set. All lower-lying states were treated as core states. The inclusion of Sb $(4p,4d)$ states in the valence set was necessary to account for non-negligible core-core overlaps due to the relatively large extension of the Sb $(4p,4d)$ wave functions. The $5d$ states were taken into account to achieve a more complete basis set. The spatial extension of the basis orbitals, controlled by a confining potential $(r/r_0)^4$, was optimized in order to minimize the total energy.[23] Brillouin-zone integrations were performed using the tetrahedron method. Convergence with respect to the basis set and the k mesh was carefully evaluated for all considered structure types.

IV. RESULTS AND DISCUSSION

A. Low-pressure phase and transition Sb-I to Sb-II

The homogeneous intensity distributions within the rings of the x-ray-diffraction patterns indicate a good powder average in samples of the low-pressure phase. Diffraction diagrams of this modification revealed no extra peaks (see Fig. 1) thus evidencing pure single-phase rhombohedral antimony as starting material. The structural parameters at a pressure of 6.4 GPa as determined from refinements using full reflection profiles are in good agreement with earlier results from single-crystal data.[24] The hydrostatic compression is accompanied by a significant decrease of the ratio c/a and an increase of the positional parameter value z. In comparison to the coordination at ambient pressure, we find at 6.4 GPa that the longer Sb-Sb distances are shortened by almost -7% whereas the shorter bonds exhibit a change of only -1%.[25] These changes are consistent with a significant reduction of the deviation of the rhombohedral $A7$ structure from a cubic primitive arrangement (see Ref. 26 for a detailed discussion).

Above 8.2(3) GPa, additional reflections which gain intensity with increasing pressure indicate the onset of a structural phase transition (Fig. 1). In direction of ascending pressures, pure patterns of the high-pressure phase Sb-II are observed above 13(1) GPa.

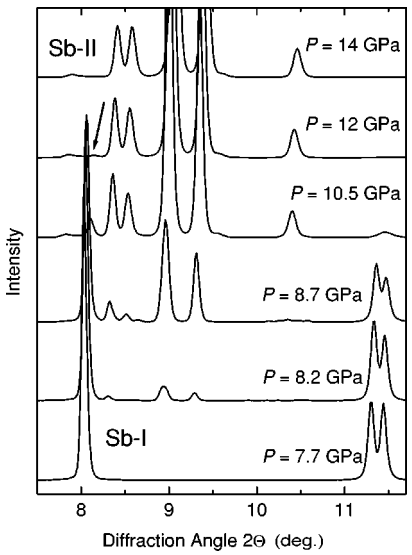

FIG. 1. Integrated x-ray-diffraction profiles of Sb-I (7.7 GPa), phase mixtures of low- and high-pressure modifications in the pressure range of the structural phase transition, and Sb-II (14 GPa). The arrow marks the reflection in the pattern measured at $P=12$ GPa, which is attributed to the strongest reflection of the low-pressure phase.

B. Structure solution and refinement of Sb-II

Analysis of the profiles reveals that several peak positions of the integrated pattern measured at $P=12$ GPa cannot be indexed on the basis of the tetragonal unit cell described earlier.[9,10] Attempts to gain a conventional three-dimensional indexing solution of the diffraction pattern using automatic procedures fail. By application of the four-index procedure for composite structures, a solution is obtained (see inset of Fig. 2) which comprises two tetragonal lattices with a common parameter a and different c axes. A least-squares refinement using 57 reflections $(hklm)$ results in $a=805.53(4)$ pm, $c_h=389.91(2)$ pm, $c_g=297.33(4)$ pm. The common lattice parameter of both substructures is labeled a, the c axis of the ''host'' sublattice formed by antimony atoms Sb_h is termed c_h, and c_g corresponds to the c axis of the ''guest'' lattice of Sb_g. The values of the lattice parameters are consistent with the findings obtained for the Sb-II structure using the pseudo-two-phase technique.[12]

Systematic extinctions are compatible with two body-centered sublattices. For the host, additional pseudoextinction conditions of reflections $(0kl0)$: $k=2n$ and $l=2n$ are possible. However, overlap with reflections of the general type $(hklm)$ does not allow a definite determination of the systematic absences and three superspace groups remain possible.[27] Besides the main reflections $(hkl0)$ and $(hk0m)$, the diffraction pattern contains weak first-order satellite reflections $(hklm)$ fulfilling the extinction condition $h+k+l+m=2n+1$ with $m=\pm 1$, and revealing a pronounced role of modulations in the crystal structure. Some weak reflections cannot be indexed as main reflections or first-order satellites. The intensities of these peaks vary at different pressures, thus disabling a definite assignment. The most

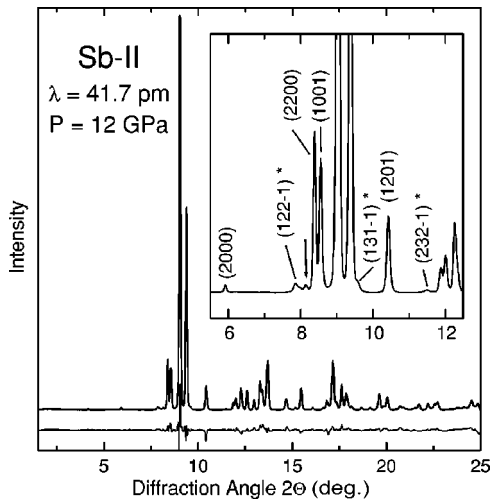

FIG. 2. Integrated x-ray-diffraction profile of Sb-II measured at $P=12$ GPa and the difference between observed and calculated intensities. The inset shows the region of the pattern exhibiting the most intense reflections ($hklm$) attributed to the modulation of atomic positions in both substructures (marked by asterisks). A single intense reflection which is tagged by an arrow is not accounted for by the host-guest structure and is attributed to be the strongest line of a residual amount of low-pressure phase Sb-I.

prominent extra reflection in the pattern at $2\Theta \approx 8.15°$ (see Figs. 1 and 2) can be unequivocally attributed to a small amount of residual low-pressure phase. In accordance with this attribution the peak has not been observed in pure Sb-II samples at higher pressure (see Fig. 1) and is also absent in an investigation performed independently.[12]

The substructure of the host atoms Sb_h was determined from the Patterson function calculated with the intensities of the ($hkl0$) reflections. The maxima are in accordance with the occupation of position $8h$ in space group $I4/mcm$, position $8j$ in $I422$, or $8c$ in $I4cm$. The substructure of the guest atoms Sb_g was established in the same way using reflections $hk0m$ and is in accordance with the twofold origin position in the three space groups $I4/mmm$, $I422$, and $I4cm$. In the three possible superspace groups, crystal structure refinements were performed using the full-profile method. In two of the three groups under consideration, first-order modulation waves of the Sb_g positions are not allowed. Thus, a complete modeling of the diffraction pattern including main reflections plus positions of the satellite reflections is performed in the superspace group $L^{I422}_{-111}:L^{I422}_{-111}$.[28] In order to calculate the intensities of the satellite reflections, the modulation functions for the Sb_h and Sb_g positions are created using a generator of the symmetry-allowed Fourier series (see Table I).[18] The structure refinement is performed in two steps. First, the average structure with the atomic parameter x_h^{av} for the Sb_h position is refined. In a second step, the intensities of the satellite reflections are taken into account in order to optimize the parameters of the modulation functions. The refinement (Fig. 2) converges at $R_{Br}=0.088$ and $R_{Pr}=0.121$. The refined coordinate $x_h^{av}=0.15776(3)$ of the Sb_h atoms corresponds well to the value of 0.1536(3) obtained for the host species in the structurally closely related modification Bi-III at 6.8 GPa.[12]

TABLE I. Positional and modulation parameters of Sb-II.

Atom site	x^{av}	y^{av}	z^{av}
Sb_h[a]	0.15776(3)	$x^{av}+1/2$	1/4
Sb_g[b]	0	0	0
Sb_h[c]	$A(1)=0.0080(1)$	$-A(1)$	$A(2)=-0.0040(2)$
Sb_h[c]	$B(1)=-0.0063(1)$	$B(1)$	
Sb_g[c]			$B(2)=0.0018(5)$

[a]Thermal displacement parameter $B_{iso}:1.85(3)\times10^4$ pm^2.
[b]Thermal displacement parameter $B_{iso}:2.75(6)\times10^4$ pm^2.
[c]$A(N)$ and $B(N)$ ($N=1,2$) are amplitudes of the modulation functions described as Fourier series. For all parameter calculations $n=1$ was used according to the order of the observed satellite reflections; the common fourth coordinate is defined as $x4=(c_h/c_g)z_h^{av}=(c_g/c_h)z_g^{av}$. Superscripts h and g indicate the host and guest atoms, respectively. Atomic coordinates of the modulated structure, e.g., x_h^{mod} are calculated using the corresponding average positional parameter x_h^{av} plus the symmetry-allowed displacement functions:

$$Sb_h: x_h^{mod}=x_h^{av}+A(1)\cos(2\pi nx4)+B(1)\sin(2\pi nx4),$$

$$y_h^{mod}=y_h^{av}-A(1)\cos(2\pi nx4)+B(1)\sin(2\pi nx4),$$

$$z_h^{mod}=z_h^{av}+A(2)\cos(2\pi nx4),$$

$$Sb_g: z_g^{mod}=z_g^{av}+B(2)\sin(2\pi nx4).$$

C. Atomic arrangement and modulation

The most intriguing feature of the Sb-II crystal structure are condensed square antiprismatic columns of Sb_h atoms forming a three-dimensional framework. This arrangement of host atoms Sb_h can be subdivided into sets of plane nets (labeled 3^2434 in Pearson notation, see Ref. 12 for details) oriented perpendicular to the c axis. However, the shortest interatomic distance in the crystal structure of Sb-II interconnects these nets to a network linked in three dimensions.

Figure 3 visualizes the crystal structure of Sb-II in two different projections. The selected representation emphasizes that the structural pattern of the host and guest atoms is commensurate in the (001) plane, while the arrangement of atoms within the channels and the resulting misfit causes incommensuration along the c axes (directions [0010] and [0001]). The same characteristic atomic arrangement as that of the host atoms in Sb-II is observed in intermetallic phases of the $CuAl_2$ type.[29,30] The capability of this structure type to adapt to different electron counts by adjustment of c/a and/or the free positional parameter x is reflected by the large variety of element combinations realizing this structural pattern.[31–33] In Sb-II, the Sb_h sublattice corresponds to the

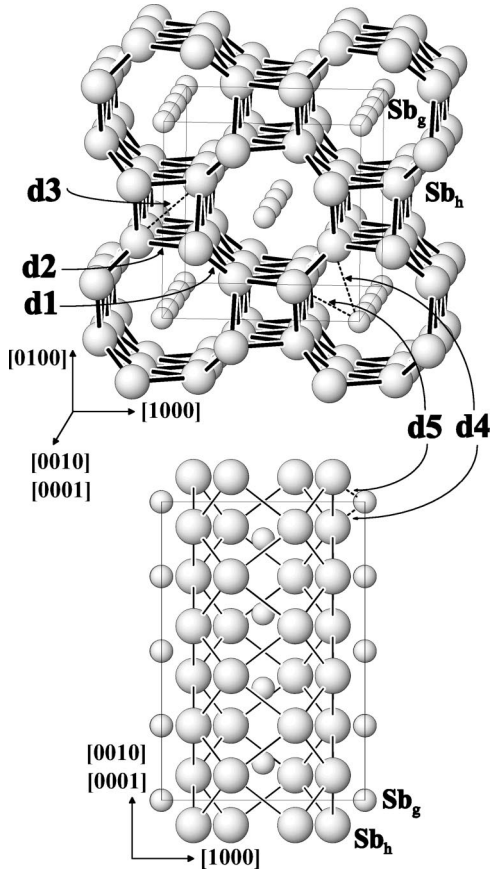

FIG. 3. Crystal structure of Sb-II shown in projections down the *c* axes (top) and along the *b* axis (bottom). Two tetragonal body-centered sublattices realize a superstructure with common *a* axes but different periodicity in the direction of the *c* axes.

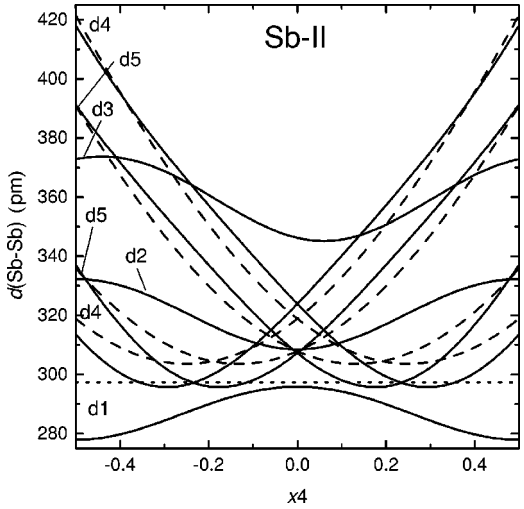

FIG. 4. Interatomic distances of Sb-II at $P=12$ GPa as a function of the fourth coordinate $x4$. Dashed lines represent distances calculated for a nonmodulated structure, full lines correspond to those of the modulated atomic arrangement, and the dotted line reproduces the distance between channel atoms.

configuration of aluminum atoms in the crystal structure of $CuAl_2$ with a surprising similarity of the positional parameter of Al ($x=0.1581$) to x_h^{av} of Sb_h.[29,30] The resulting tubular assemblies of this substructure are occupied by a body-centered arrangement of guest atoms Sb_g. However, the copper atoms in $CuAl_2$ occupy all tetragonal antiprismatic voids whereas the Sb_g sublattice contains only slightly more than half the number of atoms corresponding to $(Sb_g)_{1-x}(Sb_h)_2$ with $x\approx 0.33$. The finding of isotypic partial structures of $CuAl_2$ and antimony at high pressures confirms the importance of structural motifs of intermetallic compounds for high-density modifications of elements. The analoguous atomic organization of an intermetallic compound and the structural pattern of Sb-II indicates a pressure-induced dissimilarity of chemically identical, but structurally different atoms, which is also observed in several low-symmetry modifications of elemental metals.[34–36]

The modulation of the Sb_h atoms facilitates a continuous adjustment of interatomic distances as a function of the common fourth coordinate $x4$. For the interactions among the host and guest atoms, $d4$ and $d5$, the modulated displacement of antimony atoms induces an additional reduction in the regime of short interatomic contacts and an elongation at long distances. The distances $d3$ located within tetrahedral chains connecting the antiprisms which play a decisive role in $CuAl_2$-type structures are significantly longer than strongly bonding contacts and, thus, are not supposed to represent robust covalent interactions of atoms Sb_h. The interatomic spacing between neighboring guests within the same channel falls into the range of the majority of minimal interatomic antimony distances. This finding is taken as an indication of a pronounced influence of intrachannel interactions between antimony atoms on the lattice parameter c_g.

Every atom Sb_g has two neighbors in the channel with a distance ≈ 297 pm. Two extreme situations mark the coordination range of Sb_g: The lower limit of CN 6 is realized when the guest species is coordinated by four host atoms in the center of a square ($x4=\pm 0.5$), the upper limit of CN 10 corresponds to a location of Sb_g in the center of the square antiprisms of Sb_h ($x4=0$) as is found for the ideal Cu position in the $CuAl_2$ structure. Thus, the coordination polyhedra of Sb_g are formed by two channel atoms Sb_g plus $4(+4)$ atoms Sb_h (distances $d4$ and $d5$ in Fig. 3 and Fig. 4). The host atoms Sb_h have CN 8 and are coordinated by six framework atoms (distances $d1$ and $d2$) plus two channel atoms Sb_g ($d4$ and $d5$). The pressure-induced changes of the ratios c_h/a and c_g/a are small thus indicating that the compressibility is nearly isotropic, which evidences that the three-dimensionally connected host structure dominates the compression properties. Within the stability region of the modification Sb-II, the axial ratio c_h/c_g changes by less than 0.4% and does not achieve the next higher rational value 4/3 that would result in a commensurate structure with the smallest possible common lattice parameter *c* of the guest and host lattices. However, we will use this commensurate *approximant* of the modulated composite which reproduces the basic features of the atomic organization adequately as a model structure for the total-energy calculations.

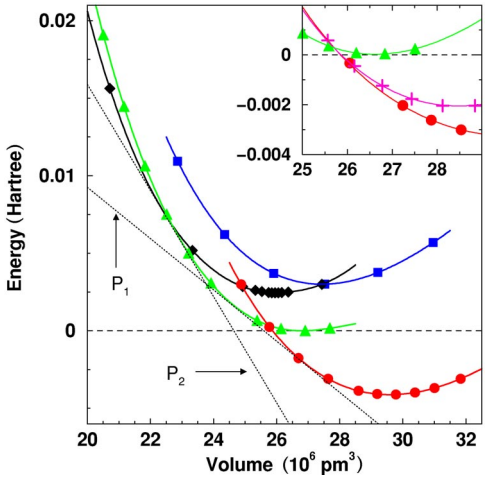

FIG. 5. Energy versus volume per atom for the different structures under investigation. The calculated energies are marked by symbols: (i) Rhombohedral ($A7$), circles; (ii) simple cubic (SC), crosses (see inset); (iii) tetragonal approximant (TA), triangles; (iv) body-centered cubic (BCC), diamonds; and (v) tetragonal primitive (TP), squares. Solid lines are cubic splines fitted to the calculated values. The dotted lines are tangents to the energy-volume curves according to the Helmholtz construction illustrating the calculated transition pressures P_1 ($A7$ to TA) and P_2 (TA to BCC).

D. The total-energy calculations

The crystal structures being considered as models in the total-energy calculations are restricted to the experimentally evidenced modifications of antimony or varieties thereof: (i) the rhombohedral structure ($A7$), (ii) simple cubic (SC; cubic primitive), (iii) an approximant of the incommensurate composite (tetragonal approximant, TA) suggested in this work, tetragonal with $P4/mcc$ symmetry, (iv) body-centered cubic (BCC), (v) the tetragonal arrangement (tetragonal primitive, TP) with $P4/n$ symmetry proposed earlier.[8] The $A7$ structure is the stable phase at ambient pressures (up to about 8.5 GPa). The simple cubic structure can be viewed as a special case of the $A7$ structure, and it was observed for the lighter group V B elements (P and As) as the modification neighbored to $A7$ at higher pressures. The BCC arrangement is the stable phase of Sb at pressures above 28 GPa. The fundamental problem that we want to address here is the structure of antimony between the $A7$ and the BCC modifications.

The results of the total-energy calculations are summarized in Fig. 5. The results concerning energy and volume are normalized by the number of atoms in the unit cell in order to facilitate a straightforward comparison of the investigated structure types. The zero energy is chosen as the energy minimum of the idealized composite (TA) with $P4/mcc$ symmetry approximating the incommensurately modulated structure proposal. The results for the two independent calculation schemes agree almost perfectly, as it is evidenced by the values for the equlibrium volumes and the corresponding energies as listed in Table II. The calculated equilibrium volumes agree within less than 1% for all investigated structure types. The corresponding total-energy differences (referred to the TA structure) agree up to several hundredth mhartree except for the $A7$ structure where we find a slight offset of both curves, probably due to numerical differences caused by the different handling of crystal symmetries in both methods. The excellent agreement of two independent methods is taken as a strong evidence for the reliability of the calculational results.

TABLE II. Comparison of the equilibrium volumes and the corresponding energies for the four structures under consideration calculated by using FPLMTO and FPLO, respectively. The zero energy is chosen with respect to the equilibrium volume of the tetragonal approximant TA.

Crystal structure	Volume (10^6 pm^3)		Energy (mhartree)	
	FPLMTO	FPLO	FPLMTO	FPLO
$A7$	29.7	29.6	−3.28	−4.12
TA	26.6	26.8	0	0
BCC	25.8	25.9	2.37	2.44
TP	27.1	27.4	3.03	3.00

In order to reduce the required computing time, the c/a ratios of the tetragonal structures are fixed to the experimental values. For the $A7$ type, we optimized the c/a ratio for the equlibrium volume and kept the value fixed in the subsequent calculations, since its influence on the total energies is negligible. In contrast, the total energy is significantly affected by changes of the positional parameter. Thus, the internal coordinate z of the $A7$ structure is optimized at each calculated point.[37] As can be seen from Fig. 5 the sequence of phase transitions predicted by the calculations is in perfect agreement with the experimental findings. At pressures up to about 8.7 GPa the $A7$ structure is stable. As shown in the inset of Fig. 5, the SC structure lies higher in energy at low pressures. The energy differences between $A7$ and the SC structure decrease with increasing pressure and become exceedingly small near the phase-transition region. In accordance with experimental results, the total-energy calculations evidence that a different crystal structure emerges before the SC arrangement becomes more stable than $A7$. For volumes less than about 22×10^6 pm^3 (corresponding to about 75% of the theoretical equilibrium volume of 29.710^6 pm^3) the BCC structure has the lowest energy, in complete accordance with the results of previous experiments. In the region between these phases, the approximant (TA) is found to be almost 3 mhartree per atom lower in energy than the crystal structure suggested earlier.[8] Consequently, the total-energy calculations definitely rule out the TP structure as a possible Sb-II modification. In order to provide a quantitative measure between experimental and theoretical findings, we show the experimental data in comparison to the theoretical pressure-volume curve (Fig. 6). The theoretical values are obtained from Birch-Murnaghan-type equations of state. Since measured and calculated volumes match almost perfectly (ambient pressure: 30.1×10^6 pm^3 versus 29.7×10^6 pm^3, respectively), both data sets are plotted by using absolute volumes rather than scaled values. The agreement between theory and experiment is excellent for the Sb-I phase ($A7$) and the

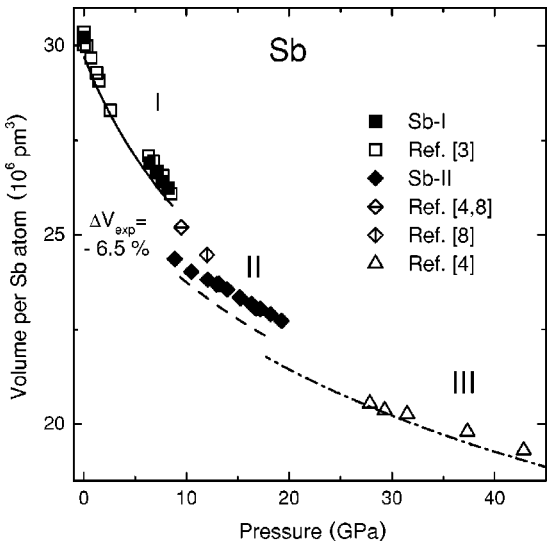

FIG. 6. Volume per antimony atom at pressures up to 42 GPa. Solid symbols represent data from the present investigation; open icons indicate values taken from literature (phases Sb-I to Sb-III). Curved lines represent the Birch-Murnaghan-type equations fitted to the results of the quantum-mechanical calculations for *A*7, TA, and BCC structures, respectively.

Sb-III modification (BCC). Note that for Sb-II, a commensurate approximant (TA) is used instead of the actual incommensurately modulated composite. Nevertheless, the transition pressure of 8.7 GPa and the volume decrease of 5.9% (with respect to theoretical volume) are in sound accord with the experimental data. The transition pressure for the second phase transition is predicted to be smaller: 17.7 GPa calculated for TA to BCC versus 28 GPa measured for Sb-II to Sb-III.[4]

E. Summary

The proposed structural model for the high-pressure phase Sb-II allows an integrated description of both main and satellite reflections in an x-ray powder-diffraction pattern of an incommensurately modulated atomic assembly of a main group element. The structure changes in antimony at high-pressures were modelled by quantum-mechanical calculations (FPLMTO and FPLO). We obtain excellent agreement between the calculated and experimentally determined sequence of structural phase transitions and pressure-volume relations. Moreover, on the basis of the calculated total energies we can discard an earlier proposed crystal structure in favor of an approximant developed on the basis of the four-dimensional model. The present investigation of Sb-II evidences that the interaction between the two incommensurate atomic arrangements in one crystal structure induces modulated atomic displacements of atoms in both sublattices and leads to a surprisingly complex structural organization of atoms in a chemical element. The structural similarity to the host-guest structures of the high-pressure modifications of bismuth, barium, and strontium indicates the importance of incommensuration and modulation for element structures. We expect that high accuracy experimental techniques for structure solution and refinement, even from x-ray powder-diffraction data, in combination with sophisticated theoretical methods will shed new light on the phase diagrams of chemical elements.

Note added. During the editorial process of our manuscript we became aware of an independently performed theoretical investigation published in December 2002.[38] In this work high-pressure structures of As, Sb, and Bi were studied by a first-principles pseudopotential method. However, a different model approximates the Sb-II phase and the earlier proposed atomic arrangement is not considered.

[1] P.W. Bridgman, Proc. Am. Acad. Arts Sci. **74**, 425 (1942).
[2] T. Sasaki, K. Shindo, and K. Niizeki, Solid State Commun. **67**, 569 (1988).
[3] D. Schiferl, D.T. Cromer, and J.C. Waber, Acta Crystallogr., Sect. B: Struct. Crystallogr. Cryst. Chem. **37**, 807 (1981).
[4] K. Aoki, S. Fujiwara, and M. Kusabe, Solid State Commun. **45**, 161 (1983).
[5] L.F. Vereschchagin and S.S. Kabalkina, Sov. Phys. JETP **20**, 274 (1965).
[6] S.S. Kabalkina, T.N. Kolobyanina, and L.F. Vereschchagin, Sov. Phys. JETP **28**, 88 (1969).
[7] M.J. Duggin, J. Phys. Chem. Solids **33**, 1267 (1972).
[8] H. Iwasaki and T. Kikegawa, High Press. Res. **6**, 121 (1990).
[9] H. Iwasaki, J.H. Chen, and T. Kikegawa, Rev. Sci. Instrum. **66**, 1388 (1995).
[10] J.H. Chen, H. Iwasaki, and T. Kikegawa, High Press. Res. **15**, 143 (1996).
[11] H. Iwasaki and T. Kikegawa, Acta Crystallogr., Sect. B: Struct. Sci. **53**, 353 (1997).
[12] M.I. McMahon, O. Degtyareva, and R.J. Nelmes, Phys. Rev. Lett. **85**, 4896 (2000).
[13] D. Singh and W.E. Pickett, Nature (London) **374**, 682 (1995).
[14] H. Rosner, S.-L. Drechsler, K. Koepernik, I. Opahle, and H. Eschrig, in *Rare Earth Transition Metal Borocarbides (Nitrides): Superconducting, Magnetic and Normal State Properties* (Kluwer Academic, Dordrecht, 2001).
[15] P. Soderlind, O. Eriksson, B. Johansson, J.M. Wills, and A.M. Boring, Nature (London) **374**, 524 (1995)
[16] H. Rosner and W.E. Pickett, Phys. Rev. B **67**, 054104 (2003).
[17] A.P. Hammersley *et al.*, High Press. Res. **14**, 235 (1996).
[18] L. Akselrud, P. Yu. Zavalii, Yu N. Grin, V.K. Pecharski, B. Baumgartner, and E. Wölfel, Mater. Sci. Forum **133–136**, 335 (1993).
[19] J.M. Wills (unpublished); J.M. Wills and B.R. Cooper, Phys. Rev. B **36**, 3809 (1987); D.L. Price and B.R. Cooper, *ibid.* **39**, 4945 (1989); J.M. Wills, O. Eriksson, and M. Alouani, in *Electronic Structure and Physical Properties of Solids: The Uses of the LMTO Method*, edited by H. Dreysse (Springer, Berlin, 2000), p. 148.
[20] K. Koepernik and H. Eschrig, Phys. Rev. B **59**, 1743 (1999).
[21] J.P. Perdew and Y. Wang, Phys. Rev. B **45**, 13244 (1992).
[22] D.J. Chadi and M.L. Cohen, Phys. Rev. B **8**, 5747 (1973); S. Froyen, *ibid.* **39**, 3168 (1989).

[23] H. Eschrig, *Optimized LCAO Method and the Electronic Structure of Extended Systems* (Springer, Berlin, 1989).

[24] $P=6.4$ GPa: $a=420.5(1)$ pm, $c=1054.5(2)$ pm; $z=0.2399(1)$; $R_I=0.046$ and $R_P=0.041$. Single-crystal results for comparison: $P=6.3$ GPa, $a=421.4(1)$ pm, $c=1056.9(1)$ pm, $z=0.2397(2)$ (Ref. 3).

[25] Ambient pressure: 290.8(4) pm and 335.5 pm.[3] 6.4 GPa: 287.7(1) pm and 312.7(1) pm.

[26] H.J. Beister, K. Strössner, and K. Syassen, Phys. Rev. B **41**, 5535 (1990).

[27] The three possible superspace groups are $L^{I422}_{-111}:L^{I422}_{-111}$, $L^{I4cm}_{111}:L^{I4mm}_{111}$, or $L^{I4/mcm}_{1-111}:L^{I4/mmm}_{1-111}$. For explanations of the symbols see: A. Yamamoto, Acta Crystallogr., Sect. A: Found. Crystallogr. **A48**, 476 (1992); A. Yamamoto, *ibid.* **A49**, 831 (1993).

[28] Equivalent positions: $(0,0,0,0;1/2,1/2,1/2,1/2)$ $+x1,x2,x3,x4$; $x1,-x2,-x3,-x4$; $-x2,-x1,-x3,-x4$; $x2,x1,-x3,-x4$; $-x1,-x2,x3,x4$; $-x1,x2,-x3,-x4$; $x2,-x1,x3,x4$; $-x2,x1,x3,x4$.

[29] J.B. Friauf, J. Am. Chem. Soc. **49**, 3107 (1927).

[30] A. Meetsma, J.L. de Boer, and S. van Smaalen, J. Solid State Chem. **83**, 370 (1989).

[31] H. Takizawa, T. Yamashita, K. Uheda, and T. Endo, Phys. Status Solidi B **223**, 35 (2001).

[32] H. Takizawa, K. Uheda, and T. Endo, J. Alloys Compd. **287**, 145 (1999).

[33] E.E. Havinga, H. Damsma, and P. Hokkeling, J. Less-Common Met. **27**, 169 (1972).

[34] U. Schwarz, A. Grzechnik, K. Syassen, I. Loa, and M. Hanfland, Phys. Rev. Lett. **83**, 4085 (1999).

[35] M.I. McMahon, S. Rehki, and R.J. Nelmes, Phys. Rev. Lett. **87**, 055501 (2001).

[36] U. Schwarz, O. Jepsen, and K. Syassen, Solid State Commun. **113**, 643 (2000).

[37] In the $A7$ structure each atom has three nearest neighbors (strong bonds) in the same plane, and three next-nearest neighbors (weak bonds) in the neighboring plane. Changing the c/a ratio affects mainly the length of the next-nearest-neighbor distance, thus it modifies only the strength of the weaker bond. On the other hand, altering the parameter z also affects the nearest-neighbor distance and changes the overlap of strongly bonded atoms.

[38] U. Häussermann, K. Söderberg, and R. Norrestam, J. Am. Chem. Soc. **124**, 15359(2002).